


Possible high-spin states in hydrogenated C_{60} molecules

Shao-Bin Qiu, Yu-Jun Zhao, Yao Yao, and Xiao-Bao Yang ^{*}

Department of Physics, South China University of Technology, Guangzhou 510640, People's Republic of China



(Received 27 May 2021; accepted 4 October 2021; published 13 October 2021)

Atoms with principal quantum number smaller than 2 are traditionally regarded to be nonmagnetic, but recent appealing advances in the understanding of ferromagnetism in materials such as graphene nanoribbons with zigzag edges and triangular graphene nanoflakes pave a novel way to investigate magnetism in materials merely with s and p orbitals. Opening the p shell turns out to be essential for the production of unpaired electrons, and the normal chemical treatment is to modify the molecules with various atoms and groups such as hydrogen. In this paper, we combine first-principles calculations with the Hubbard model to investigate magnetic properties in hydrogenated C_{60} ($C_{60}H_n$). For the enumerated $C_{60}H_2$ structures, there are nine configurations with ferromagnetic ground states and one configuration with an antiferromagnetic ground state. We have proposed a pair magnetic interaction model to predict the magnetic order, as well as a general rule to screen the maximum local magnetic moments for given n . When $n = 3$ and 4, our model can give a good prediction of magnetic order, which is confirmed by the first-principles calculations. We find that the maximum number of unpaired electrons in $C_{60}H_n$ is smaller than the number of hydrogen atoms when $n \geq 6$.

DOI: [10.1103/PhysRevB.104.134409](https://doi.org/10.1103/PhysRevB.104.134409)

I. INTRODUCTION

Traditional magnetic materials have important applications in high-performance memory and magnetic sensors, and the electrical switching and multistable magnetic memory effect in antiferromagnets expand the application in spintronics [1,2]. In general, the magnetism in solids is related to the existence of transition metal elements with d electrons and rare earth elements with f electrons. The magnetic force microscopy of graphite with proton irradiation showed that magnetism could also appear in materials only composed of elements with sp electrons [3,4], which had stimulated experimental and theoretical studies on magnetic order in carbon materials. For example, antiferromagnetic (AFM) order will appear in graphene nanoribbons with zigzag edges [5–7], and the triangular graphene nanoflakes and nanoholes in graphene have been predicted to have a large number of magnetic moments [8–10]. Recently, great breakthroughs have been achieved in the accurate on-surface synthesis of graphene nanostructures, which make it possible to design the molecule with a high-spin state and modulate the magnetic exchange coupling strength [11–14]. Moreover, the topological tailoring of graphene nanostructures can achieve excellent quantum properties, and the spin coherence time exceeds that of most nanomaterials [15]. Compared with transition metal materials, the organic materials which only contain light p -block elements have excellent properties such as low density, high biocompatibility, and strong plasticity [16], indicating the possibility of quantum coherence control for the next generation of carbon-based optoelectronic, electric, and bioactive systems [15].

Similar to the graphene nanostructures, the sp^2 hybridization is dominant in the buckyball fullerene [isolated-pentagon rule (IPR) C_{60}], which can be polymerized under the irradiation of charged particle beams. Experiments show that the polymerized C_{60} in the presence of oxygen can be ferromagnetic (FM) at room temperature and higher temperatures [17,18]. In pure organic molecular magnets, TDAE- C_{60} [where TDAE is tetrakis(dimethylamino)ethylene] exhibits an abnormally high Curie temperature (16 K) during ferromagnetic transition [19]. Since there is no magnetism in the perfect C_{60} , the discovery of ferromagnetism in polymerized C_{60} should be attributed to the structural defects induced by chemical adsorption or substitution [20,21]. Among various adsorption atoms and ligands, theoretical study showed that hydrogen was the best dopant to induce high-spin states in C_{60} due to the complete charge transfer [22]. Theoretical calculations have shown that the magnetic moment of one $C_{60}H_n$ molecule could be only $1 \mu_B$ or 0, corresponding to n being odd or even, respectively [21]. The hydrogenated C_{60} tends to form compounds without magnetic order such as $C_{60}H_{24}$ and $C_{60}H_{36}$ [23,24]. However, observations of large spins in graphene nanoflakes with even electrons [13,14] indicate that the distribution of hydrogen on C_{60} will effectively modulate the magnetic order.

The systematical research of magnetic properties in C_{60} derivatives requires an accurate and fast estimate of magnetic order for the given structures. For the graphene nanostructures composed of two sets of sublattices (A and B), Lieb's theorem [25] pointed out that the spin angular momentum in the ground state could be predicted as $S = \frac{1}{2}||A| - |B||$, indicating that the system presents a high-spin ground state when the number of A sites and the number of B sites are different. However, Lieb's theorem is no longer applicable to the system of $C_{60}H_n$, because the system cannot be divided

^{*}scxbyang@scut.edu.cn

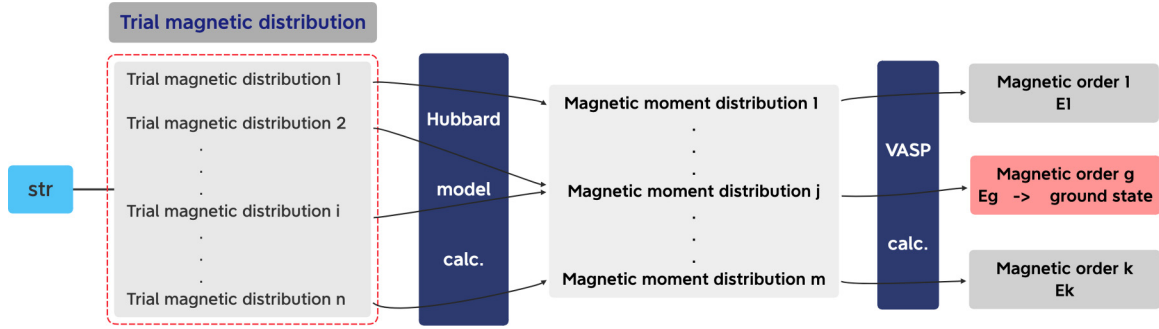


FIG. 1. Workflow of $C_{60}H_n$ calculations: Combining the first-principles calculations with the Hubbard model, we can determine the magnetic states and their energies for a given structure (str).

into two sublattices as a result of the existence of pentagons. To determine the magnetic ground state of $C_{60}H_n$, the first-principles calculations with spin polarization can be adopted, and the results usually depend on the initial magnetic moment setting.

In this paper, we have studied the magnetic properties of C_{60} with the adsorption of various hydrogen atoms, in order to understand the room temperature ferromagnetic mechanism of polymerized C_{60} . Combining the first-principles calculations with the Hubbard model, we have determined the magnetic ground state of the enumerated $C_{60}H_2$ and proposed a general rule to screen the maximum magnetic moments for given n . As a result, the maximum number of unpaired electrons is smaller than the number of hydrogen atoms when $n \geq 6$.

II. METHOD

Generally, exact diagonalization (ED) will give an accurate result, although it is difficult to apply in large systems such as hydrogenated C_{60} , due to the overly expensive cost. A previous study showed that the difference between mean-field theory (MFT) and exact diagonalization in the graphene system can be acceptable, including the energy, gap, and magnetic moment [26]. Recent experimental observations confirmed the charge distributions which have been predicted by the mean-field Hubbard model and first-principles calculations [27–30]. To enhance the efficiency, we judge whether the system will have magnetic order by the mean-field Hubbard model, which also provides the distribution of local magnetic moment in hydrogenated C_{60} .

To determine the magnetic ground state of a given structure, the workflow of combining the first-principles calculations with the Hubbard model is showed in Fig. 1. Generally, only a few magnetic orders could stably exist, whereas there are plenty of possible initial distributions for magnetic moment to be considered. To reduce the amount of time consumed by the first-principles calculations, we have screened various trial magnetic distributions with the Hubbard model, determining the magnetic orders which could maintain stability. Finally, we confirm the magnetic ground state based on the first-principles calculations, in which the initial distributions of local magnetic moment are from the results of the Hubbard model.

The first-principles calculations are performed using the Vienna *ab initio* simulation package (VASP) [31,32]. The Perdew-Burke-Ernzerhof generalized gradient approximation (GGA) is applied [33,34]. The energy cutoff of the plane wave is 600 eV, the convergence criterion of the energy is 1×10^{-5} eV, and the forces acting on each atom are less than 1 meV/Å in self-consistent calculations. The size of the vacuum layer is 12 Å, and the k -point sheet is $1 \times 1 \times 1$.

The electronic properties of sp^2 carbon materials can be described accurately by the Hubbard model [28]. The mean-field Hubbard Hamiltonian

$$H_{MF} = -t \sum_{\langle i,j \rangle, \sigma} c_{i\sigma}^\dagger c_{j\sigma} + U \sum_i (n_{i\uparrow} \langle n_{i\downarrow} \rangle + \langle n_{i\uparrow} \rangle n_{i\downarrow} - \langle n_{i\uparrow} \rangle \langle n_{i\downarrow} \rangle), \quad (1)$$

where $c_{i\sigma}^\dagger$ and $c_{i\sigma}$ are the creation operator and the annihilation operator with spin σ ($\sigma = \uparrow, \downarrow$) at site i , respectively, t is the hopping integral between the nearest-neighbor sites i and j , and $n_{i\sigma}$ is the spin-resolved electron density at site i . The second term is the Coulomb interaction energy. It goes through all sites and adds an energy U to H_{MF} for the doubly occupied sites. $\langle n_{i\sigma} \rangle$ is the average spin-resolved electron population at site i . The local magnetic moment of site i is

$$M_i = \frac{\langle n_{i\uparrow} \rangle - \langle n_{i\downarrow} \rangle}{2}. \quad (2)$$

The values of t and U depend on the choice of the exchange-correlation functional within the first-principles calculations. Here, we use $t = 2.5$ eV and $U = 1.3t$ [35].

III. RESULTS AND DISCUSSION

In the following, we first illustrate the distributions of hydrogen atoms and magnetic properties of $C_{60}H$ and $C_{60}H_2$ isomers in Sec. III A. In Sec. III B, we show the details of the pair magnetic interaction model and provide the rule for screening the isomers with large spins. In addition, the relationship between the total magnetic moments and the configurations of $C_{60}H_n$ ($n = 3-7$) is discussed.

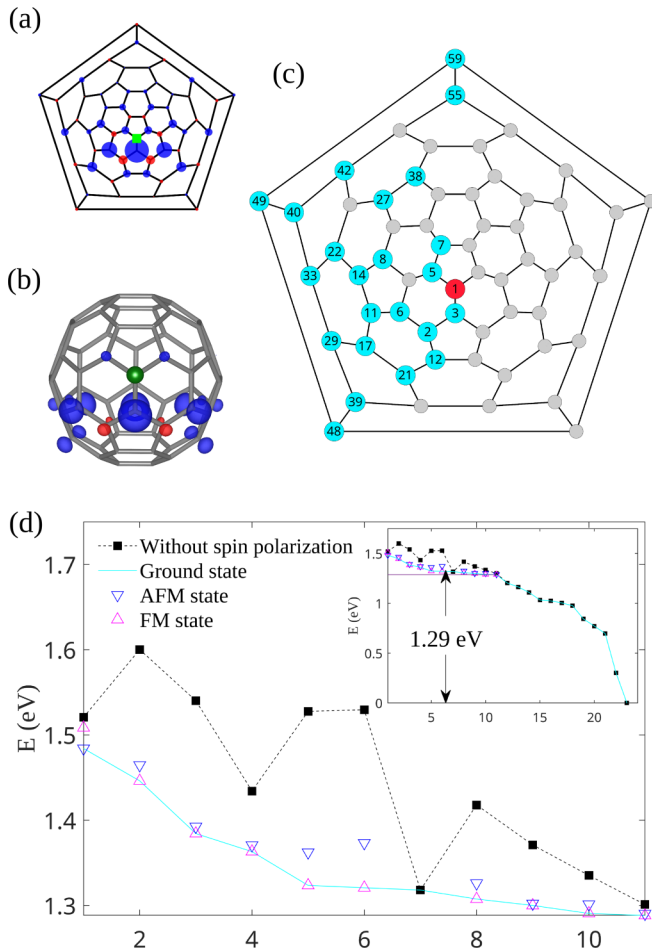


FIG. 2. The spin distributions in $C_{60}H$: (a) results from the Hubbard model calculations; (b) results from first-principles calculations. Blue (red) isosurfaces correspond to spin-up (spin-down) densities. The area of the circle stands for the value of the spin density. The structures and energies of $C_{60}H_2$ isomers: (c) structures of $C_{60}H_2$ (the red site and any one of the light cyan sites are the adsorption sites of $C_{60}H_2$); (d) the energies of $C_{60}H_2$ with different magnetic states from first-principles calculations. The inset shows the energies of 23 $C_{60}H_2$ isomers

A. Magnetic ground states of $C_{60}H_2$ isomers

When a hydrogen atom is adsorbed on the surface of C_{60} , the formation of the C-H bond will induce sp^3 hybridization at the four-coordinate carbon atom, and the number of π electrons in the system is odd. The adsorption of the hydrogen atom makes one orbit far away from the Fermi level and produces an orbit near the Fermi level, which can only be occupied by a single electron due to the Coulomb interaction. Thus the ground state of $C_{60}H$ will be magnetic due to this unpaired electron. Figures 2(a) and 2(b) show the spin distribution of $C_{60}H$ from the Hubbard model and the first-principles calculations, respectively.

There is almost no spin density distributed around the carbon atom connected with the hydrogen atom; the spin density is mainly concentrated around the carbon atom at the other end of the hexagonal-hexagonal C-C bond, and the second-largest electron cloud is distributed on the two

hexagons opposite to the adsorption site. Obviously, the result from the Hubbard model is consistent with the one from the first-principles calculations, indicating that the magnetic hydrogenated C_{60} can be screened by the Hubbard model.

It is generally believed that the system with an even number of electrons will not show magnetic properties because there are no unpaired electrons. Thus the system contains no more than one unpaired electron when the number of adsorbed hydrogen atoms is odd, and the magnetic moment of hydrogenated C_{60} will not exceed $1 \mu_B$ [21]. In the following, we focus on $C_{60}H_2$ with magnetic moment equal to $2 \mu_B$, where all the isomers of hydrogenated C_{60} can be obtained from the Structures of Alloy Generation and Recognition (SAGAR) software package [36] by removing the duplicate structures. Due to the symmetry of the molecule, there are only 23 nonequivalent structures for $C_{60}H_2$, as shown in Fig. 2(c).

The inset of Fig. 2(d) shows the structural stabilities of all the $C_{60}H_2$ isomers, and the H2(1,3) [H2(i, j) represents the structure with adsorption sites i and j in Fig. 2(c)] has the lowest energy, in good agreement with previous studies [20,21]. The total energy of H2(1,3) is lower by 0.8665 eV than that with the isolated C_{60} and H_2 molecule. When there are two H atoms adsorbing on the (1,22) sites, the ground state of this structure is at a high-spin state. Though the energy of H2(1,22) is 1.29 eV higher than the energy of H2(1,3), the hydrogen atoms will be captured due to the strong C-H bonds, and the magnetic isomer of $C_{60}H_2$ is expected to be dynamically stable. For structures with large spins, the structural stability can be enhanced by the substrate, and the magnetic carbon materials have been fabricated by the on-surface synthesis approach [37–39].

According to the Hubbard model, we found that there are 14 structures with magnetic order and there are no local magnetic moments in the other nine structures. Among the 14 structures, the first-principles calculations show that the ground states of nine structures are ferromagnetic and the ground state of one is antiferromagnetic. The total magnetic moment of each of the ferromagnetic structures is $2 \mu_B$, and that of the antiferromagnetic one is 0. Note that the calculated energy of a given $C_{60}H_2$ can be overestimated when the distribution of local magnetic moments is not set properly. As shown in Table I, the maximum energy difference between the FM and nonmagnetic (NM) states is 208.8 meV in the structure H2(1,48), and the energy difference between the AFM and NM states will reach 165.4 meV.

The above results show that there is a difference between the first-principles calculations and the Hubbard model. There is only one parameter in the Hubbard model, and thus its total energy calculation of $C_{60}H_n$ is not accurate compared with first-principles calculations. In general, the energy difference between the FM state and the AFM state is small, and it is difficult to estimate this energy difference using the Hubbard model. Therefore we start with the magnetic orders from the Hubbard model and perform the first-principles calculations to obtain the total energy with higher accuracy.

Only when two hydrogen atoms adsorb at the metapositions in the pentagon [H2(1,7)] is the magnetic ground state AFM, and the energy difference between the FM state and

TABLE I. In $C_{60}H_2$ isomers, the energy difference between the FM state and the AFM state ($E_{FM} - E_{AFM} = \Delta E_1$), the energy difference between the AFM state and the NM state ($E_{AFM} - E_{NM} = \Delta E_2$), the energy difference between the FM state and the NM state ($E_{FM} - E_{NM} = \Delta E_3$), and the energy difference between the FM state and H2(1,3) ($E_{FM} - E_{H2(1,3)} = \Delta E_4$). $\Delta E_1 > 0$ indicates the ground state of the AFM magnetic configuration, corresponding to a total magnetic moment of 0. $\Delta E_1 < 0$ indicates the FM ground state with a total magnetic moment of $2 \mu_B$.

Sites	ΔE_1 (meV)	ΔE_2 (meV)	ΔE_3 (meV)	ΔE_4 (eV)
(1,7)	24.4	-36.6	-12.2	1.5084
(1,48)	-52.6	-156.4	-208.8	1.3206
(1,40)	-38.8	-165.4	-204.2	1.3234
(1,59)	-18.6	-135.6	-154.1	1.4460
(1,38)	-18.6	-92.0	-110.5	1.3074
(1,22)	-10.6	-33.9	-44.6	1.2905
(1,2)	-8.2	-147.7	-155.9	1.3842
(1,29)	-7.6	-63.4	-71.0	1.3630
(1,39)	-2.2	-68.8	-71.0	1.2998
(1,21)	-2.2	-10.7	-12.9	1.2880

the AFM state is equal to -24.4 meV. For those structures with ferromagnetic ground states, the energy differences between the FM state and the AFM state range from 2.2 to 52.6 meV, depending on the distributions of the H atoms. The first radical bow-tie nanographene, also called Clar's goblet, which holds two unpaired electrons with an antiferromagnetic coupled ground state, was synthesized recently [28]. In the structure H2(1,48), the coupling strength $J = \frac{1}{2}(E_{FM} - E_{AFM})$ can reach -26 meV, and its absolute value is larger than 23 meV in Clar's goblet. H2(1,40) has the second largest absolute value of exchange coupling strength, which is equal to -19.4 meV. In these two structures, we found that the distance between the two adsorption sites is larger than 6 Å, reflecting the existence of long-range coupling between these local magnetic moments.

Figure 3 shows the spin distributions of H2(1,48) in FM and AFM states, as well as the energy spectrum. For the FM state, the spin distribution can be composed of two spin distributions in $C_{60}H$ (shown in Fig. 2) with the same direction. By spin-flipping one of the spin distributions, the spin distribution of the AFM state can be obtained. According to the energy spectrum from the calculations with or without spin polarization, it is found that the appearance of magnetic order is attributed to the competition between Coulomb interaction and spin pairing. Without spin polarization, the highest occupied molecular orbital (HOMO) and the lowest unoccupied molecular orbital (LUMO) of H2(1,48) are almost degenerate. Considering the spin polarization, there are two extra electrons in the spin-up orbitals compared with the spin-down orbitals, corresponding to the FM state. The energy levels of two occupied spin-up orbitals are reduced by about 180 meV, and the energy levels of the corresponding two unoccupied spin-down orbitals are raised, resulting in a gap of 414 meV. For the AFM state, spin-up orbitals and spin-down orbitals are completely overlapping. The energy level of the HOMO

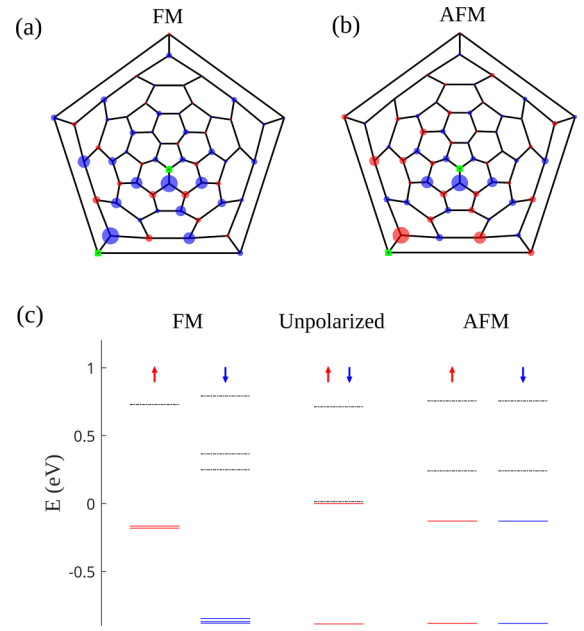


FIG. 3. Spin distributions and energy spectrum of H2(1,48). (a) Spin distribution of H2(1,48) with FM state. (b) Spin distribution of H2(1,48) with AFM state. Blue (red) isosurfaces correspond to spin-up (spin-down) densities. The area of the circles stands for the value of the spin density. (c) The energy spectrum of H2(1,48). The middle part is the spectrum from the non-spin-polarized calculation, and the left side and right side are spin-polarized calculation results with FM and AFM state, respectively. The black dashed (red or blue solid) lines denote unoccupied (occupied) molecular orbitals.

is reduced by about 128 meV, with a HOMO-LUMO gap of 370 meV.

B. Screening hydrogenated C_{60} with large spins

Because the synthesis difficulty will increase with the increase in the number of adsorbed atoms, we focus on the $C_{60}H_n$ structures whose total molecular magnetic moments (the sum of the local magnetic moments) are equal to n , defined as full magnetic moment structures (FMMSs). For a given $C_{60}H_n$, the magnetic interaction in the system can be predicted by an energy model:

$$E = \sum_{i < j} \sum J_{ij}(s_i s_j),$$

where s_i is the effective spin when one H atom adsorbs at the i site and $J_{ij}(s_i s_j)$ is the pair magnetic interaction between the i site and the j site when the effective spins are s_i and s_j , respectively. The values of s_i can be $-1, 0, 1$, and $s_i s_j = 1, 0, -1$ corresponds to the FM, NM, and AFM states, respectively. The parameters $J_{ij}(s_i s_j)$ can be obtained from Table I, and E_{NM} is set to be zero for each H2(i, j) structure. For the 13 $C_{60}H_2$ structures which are not listed in Table I, the systems will become nonmagnetic with the initialization of various magnetic states. Thus the FM and AFM states will not occur in these 13 $C_{60}H_2$ structures, and the energy differences are set to be 1 eV.

Based on the structural recognition from SAGAR [36], there are 303 and 4190 isomers for $C_{60}H_3$ and $C_{60}H_4$, respectively.

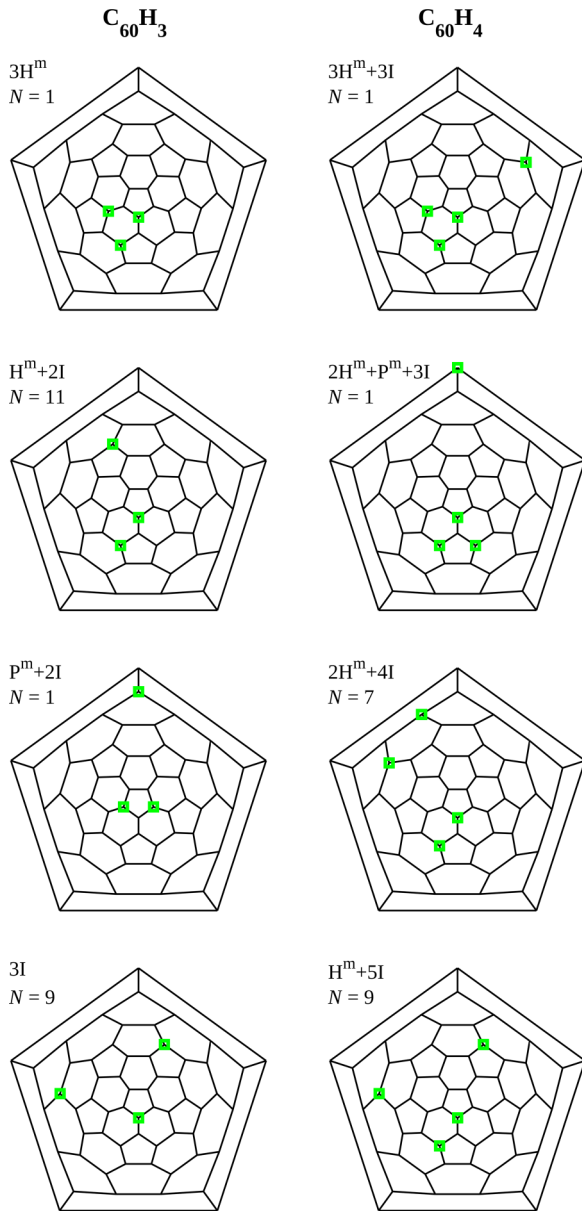


FIG. 4. Full magnetic moment structures in $C_{60}H_3$ and $C_{60}H_4$ isomers. N is the number of structures belonging to a type. The green sites are the adsorption sites.

The Hubbard model analysis shows that there are 79 FMMSs among the $C_{60}H_3$ isomers, and our energy model indicates that the number of FMMSs can be reduced to 33. According to the first-principles calculations, there are only 22 structures with total magnetic moments of $3 \mu_B$, all included in the 33 structures predicted by the magnetic interaction model. Similarly, there are 126 FMMSs in $C_{60}H_4$ isomers predicted by the Hubbard model, and the number is reduced to 60 based on the magnetic pair interaction model. Only 18 FMMSs are confirmed by the first-principles calculations, which are all included in the results from the magnetic interaction model. Compared with the Hubbard model, the magnetic interaction model can screen the FMMSs in $C_{60}H_3$ and $C_{60}H_4$ more efficiently, as confirmed by the first-principles calculations.

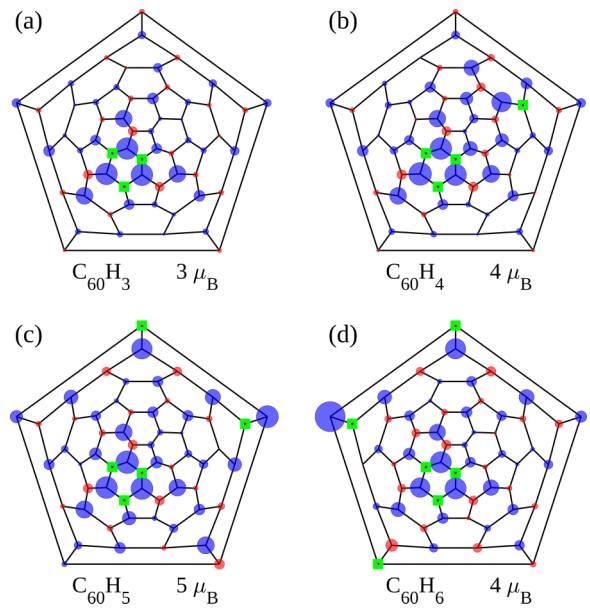


FIG. 5. (a)–(d) The spin distributions of $C_{60}H_n$, $n = 3, 4, 5, 6$, from the first-principles calculations. Blue (red) isosurfaces correspond to spin-up (spin-down) densities. The area of the circle stands for the value of the spin density.

Here, we define the pair adsorption sites on the metapositions of a hexagon as H^m , and we similarly define P^m as the pair adsorption sites on the metapositions of a pentagon. If the hydrogen pairs are not on the same pentagon or hexagon, the H atoms are considered to be isolated, and this kind of pair is defined as “I.” The number of adsorption site pairs is 3 and 6 in $C_{60}H_3$ and $C_{60}H_4$, respectively.

As shown in Fig. 4, the FMMSs in $C_{60}H_3$ can be divided into four categories according to the composition of adsorption site pairs: $3H^m$, H^m+2I , P^m+2I , and $3I$. The metapositions are required when the two hydrogen atoms are on the same pentagon or hexagon. There are nine structures of $3I$ type, in which hydrogen atoms are dispersed. Similarly, the FMMSs in $C_{60}H_4$ also can be divided into four categories: $3H^m+3I$, $2H^m+P^m+3I$, $2H^m+4I$, and H^m+5I . However, the maximum magnetic moment in the $6I$ type of $C_{60}H_4$ cannot reach $4 \mu_B$, indicating the importance of H^m pair sites for maintaining large spins. Note that the P^m type in $C_{60}H_2$ corresponds to the AFM ground state, while the P^m+2I type in $C_{60}H_3$ and $2H^m+P^m+3I$ type in $C_{60}H_4$ maintain the FM ground states, implying that the hydrogen dispersion will also induce large spins.

With the increase in n , the number of $C_{60}H_n$ isomers will grow exponentially, and the screening of FMMSs will become unacceptable using either the Hubbard model or the magnetic interaction model. According to our pair magnetic interaction model, the parameters for the nonmagnetic $C_{60}H_2$ structures are much larger than those for FM or AFM isomers, and the total magnetic moment of $C_{60}H_n$ structures will not reach $n \mu_B$ if there is a pair of adsorption sites in $C_{60}H_n$ corresponding to the sites in nonmagnetic $C_{60}H_2$. Thus a general rule can be proposed to screen the FMMSs of $C_{60}H_n$ isomers: The candidates can only be composed by the pairs of adsorption sites listed in Table I. Based on this constraint, the number of

$C_{60}H_n$ structures will decrease dramatically, and no candidate can be found when $n > 7$.

The numbers of possible FMMSs for $C_{60}H_n$ with $n = 5, 6$, and 7 are $84, 42$, and 6 , respectively. According to the first-principles calculations, we find that the FMMSs in the $C_{60}H_n$ system cannot appear when $n > 5$.

Figure 5 shows the spin distributions of typical $C_{60}H_n$, $n = 3, 4, 5, 6$, structures with the ferromagnetic ground state. All of these four structures contain a motif of $3H^m$, inducing a similar spin distribution around this triangle region. Compared with $C_{60}H_3$, the fourth hydrogen atom in $C_{60}H_4$ is isolated, and another two hydrogen atoms are on the meta-positions of the hexagon in $C_{60}H_5$. In $C_{60}H_6$, the maximum magnetic moment can reach $4 \mu_B$, and the spin distribution of one example is shown in Fig. 5(d).

IV. CONCLUSION

In summary, we have systematically investigated the magnetic properties of $C_{60}H_n$, using the mean-field Hubbard model combined with first-principles calculations. When

$n = 2-5$, we have determined the magnetic ground states of some $C_{60}H_n$ isomers, in which the total magnetic moments are equal to $n \mu_B$. With a general rule from the pair magnetic interaction model, we can conclude that the maximum number of unpaired electrons is smaller than the number of hydrogen atoms when $n \geq 6$. Note that the absolute value of the coupling strength in $C_{60}H_2$ can reach a maximum of 26 meV , which is larger than the 23 meV of Clar's goblet. Our work provides the high-spin ground states in $C_{60}H_n$ and explores the possibility of C_{60} -based spintronics.

ACKNOWLEDGMENTS

This work was supported by Guangdong Basic and Applied Basic Research Foundation (Grant No. 2021A1515010328), Key-Area Research and Development Program of Guangdong Province (Grant No. 2020B010183001), Guangdong-Hong Kong-Macao Joint Laboratory of Optoelectronic and Magnetic Functional Materials (Grant No. 2019B121205002) and National Natural Science Foundation of China (Grant No. 91833305, 11974118).

- [1] N. L. Nair, E. Maniv, C. John, S. Doyle, J. Orenstein, and J. G. Analytis, *Nat. Mater.* **19**, 1036 (2020).
- [2] A. Little, C. Lee, C. John, S. Doyle, E. Maniv, N. L. Nair, W. Chen, D. Rees, J. W. Venderbos, R. M. Fernandes, J. G. Analytis, and J. Orenstein, *Nat. Mater.* **19**, 1062 (2020).
- [3] P. Esquinazi, D. Spemann, R. Höhne, A. Setzer, K. H. Han, and T. Butz, *Phys. Rev. Lett.* **91**, 227201 (2003).
- [4] H. Ohldag, T. Tylliszczak, R. Höhne, D. Spemann, P. Esquinazi, M. Ungureanu, and T. Butz, *Phys. Rev. Lett.* **98**, 187204 (2007).
- [5] Y. W. Son, M. L. Cohen, and S. G. Louie, *Nature (London)* **444**, 347 (2006).
- [6] P. Cui, Q. Zhang, H. Zhu, X. Li, W. Wang, Q. Li, C. Zeng, and Z. Zhang, *Phys. Rev. Lett.* **116**, 026802 (2016).
- [7] R. Ortiz, J. L. Lado, M. Melle-Franco, and J. Fernández-Rossier, *Phys. Rev. B* **94**, 094414 (2016).
- [8] J. Fernández-Rossier and J. J. Palacios, *Phys. Rev. Lett.* **99**, 177204 (2007).
- [9] W. L. Wang, S. Meng, and E. Kaxiras, *Nano Lett.* **8**, 241 (2008).
- [10] X. Y. Cui, R. K. Zheng, Z. W. Liu, L. Li, B. Delley, C. Stampfl, and S. P. Ringer, *Phys. Rev. B* **84**, 125410 (2011).
- [11] G. Z. Magda, X. Jin, I. Hagymási, P. Vancsó, Z. Osváth, P. Nemes-Incze, C. Hwang, L. P. Biró, and L. Tapasztó, *Nature (London)* **514**, 608 (2014).
- [12] P. Ruffieux, S. Wang, B. Yang, C. Sánchez-Sánchez, J. Liu, T. Dienel, L. Talirz, P. Shinde, C. A. Pignedoli, D. Passerone, T. Dumslaff, X. Feng, K. Müllen, and R. Fasel, *Nature (London)* **531**, 489 (2016).
- [13] R. Ortiz and J. Fernández-Rossier, *Prog. Surf. Sci.* **95**, 100595 (2020).
- [14] J. Liu and X. Feng, *Angew. Chem., Int. Ed.* **59**, 23386 (2020).
- [15] F. Lombardi, A. Lodi, J. Ma, J. Liu, M. Slota, A. Narita, W. K. Myers, K. Müllen, X. Feng, and L. Bogani, *Science* **366**, 1107 (2019).
- [16] K. Feron, R. Lim, C. Sherwood, A. Keynes, A. Brichta, and P. C. Dastoor, *Int. J. Mol. Sci.* **19**, 2382 (2018).
- [17] Y. Murakami and H. Suematsu, *Pure Appl. Chem.* **68**, 1463 (1996).
- [18] F. J. Owens, Z. Iqbal, L. Belova, and K. V. Rao, *Phys. Rev. B* **69**, 033403 (2004).
- [19] P. M. Allemand, A. Khemani, K. C. Frisch, F. Wudl, K. Holczer, S. Donovan, G. Grüner, and J. D. Thompson, *Science* **253**, 301 (1991).
- [20] T. L. Makarova, I. B. Zakharova, O. E. Kvyatkovskii, S. G. Buga, A. P. Volkov, and A. L. Shelankov, *Phys. Status Solidi B* **246**, 2778 (2009).
- [21] K. W. Lee and C. E. Lee, *Phys. Rev. Lett.* **106**, 166402 (2011).
- [22] O. E. Kvyatkovskii, I. B. Zakharova, A. L. Shelankov, and T. L. Makarova, *Phys. Rev. B* **72**, 214426 (2005).
- [23] R. Dorel, P. de Mendoza, P. Calleja, S. Pascual, E. González-Cantalapiedra, N. Cabello, and A. M. Echavarren, *Eur. J. Org. Chem.* **2016**, 3171 (2016).
- [24] R. Ghafouri and M. Anafcheh, *Fullerenes, Nanotubes, Carbon Nanostruct.* **23**, 40 (2015).
- [25] E. H. Lieb, *Phys. Rev. Lett.* **62**, 1201 (1989).
- [26] H. Feldner, Z. Y. Meng, A. Honecker, D. Cabra, S. Wessel, and F. F. Assaad, *Phys. Rev. B* **81**, 115416 (2010).
- [27] Y. Zheng, C. Li, Y. Zhao, D. Beyer, G. Wang, C. Xu, X. Yue, Y. Chen, D.-D. Guan, Y.-Y. Li, H. Zheng, C. Liu, W. Luo, X. Feng, S. Wang, and J. Jia, *Phys. Rev. Lett.* **124**, 147206 (2020).
- [28] S. Mishra, D. Beyer, K. Eimre, S. Kezilebieke, R. Berger, O. Gröning, C. A. Pignedoli, K. Müllen, P. Liljeroth, P. Ruffieux, X. Feng, and R. Fasel, *Nat. Nanotechnol.* **15**, 22 (2020).
- [29] Y. Zheng, C. Li, C. Xu, D. Beyer, X. Yue, Y. Zhao, G. Wang, D. Guan, Y. Li, H. Zheng, C. Liu, J. Liu, X. Wang, W. Luo, X. Feng, S. Wang, and J. Jia, *Nat. Commun.* **11**, 6076 (2020).
- [30] S. Mishra, D. Beyer, R. Berger, J. Liu, O. Gröning, J. I. Urgel, K. Müllen, P. Ruffieux, X. Feng, and R. Fasel, *J. Am. Chem. Soc.* **142**, 1147 (2020).
- [31] G. Kresse and J. Furthmüller, *Phys. Rev. B* **54**, 11169 (1996).

- [32] G. Kresse and D. Joubert, [Phys. Rev. B](#) **59**, 1758 (1999).
- [33] J. P. Perdew, K. Burke, and M. Ernzerhof, [Phys. Rev. Lett.](#) **77**, 3865 (1996).
- [34] J. P. Perdew, K. Burke, and M. Ernzerhof, [Phys. Rev. Lett.](#) **80**, 891 (1998).
- [35] L. Pisani, J. A. Chan, B. agontanari, and N. M. Harrison, [Phys. Rev. B](#) **75**, 064418 (2007).
- [36] C.-C. He, J.-H. Liao, S.-B. Qiu, Y.-J. Zhao, and X.-B. Yang, [Comput. Mater. Sci.](#) **193**, 110386 (2021).
- [37] J. Y. Lee and M. H. Kang, [Phys. Rev. B](#) **75**, 125305 (2007).
- [38] S. Suto, K. Sakamoto, D. Kondo, T. Wakita, A. Kimura, A. Kakizaki, C.-W. Hu, and A. Kasuya, [Surf. Sci.](#) **438**, 242 (1999).
- [39] J. Y. Lee, J.-H. Cho, and M. H. Kang, [ChemPhysChem](#) **10**, 334 (2009).